ACS APPLIED MATERIALS & INTERFACES

Research Article

Cite This: ACS Appl. Mater. Interfaces 2017, 9, 43490−43497

www.acsami.org

Label-Free and Recalibrated Multilayer MoS_2 Biosensor for Point-of-Care Diagnostics

Heekyeong Park,[†] Gyuchull Han,[‡] Sang Woo Lee,[§] Hyungbeen Lee,[§] Seok Hwan Jeong,[†] Muhammad Naqi,[†] AbdulAziz AlMutairi,[‡] Young Jun Kim,[∥] Joonhyung Lee,[†] Wan-joong Kim,[∥] Sunkook Kim,*[,†] Youngki Yoon,*[,‡] and Geonwook Yoo*[,⊥]

[†]School of Advanced Materials Science and Engineering, Sungkyunkwan University, Suwon, Kyunggi-do 16419, Republic of Korea

[‡]Department of Electrical and Computer Engineering & Waterloo Institute for Nanotechnology (WIN), University of Waterloo, Waterloo, Ontario N2L 3G1, Canada

[§]Department of Biomedical Engineering, Yonsei University, Wonju, Gangwon-do 26493, Republic of Korea

[∥]Medical-Device Lab, Electronics and Telecommunications Research Institute, Daejeon 34129, Republic of Korea

[⊥]School of Electronic Engineering, Soongsil University, Seoul 06978, Republic of Korea

Supporting Information

ABSTRACT: Molybdenum disulfide (MoS_2) field-effect transistor (FET)-based biosensors have attracted significant attention as promising candidates for highly sensitive, label-free biomolecule detection devices. In this paper, toward practical applications of biosensors, we demonstrate reliable and quantitative detection of a prostate cancer biomarker using the MoS_2 FET biosensor in a nonaqueous environment by reducing nonspecific molecular binding events and realizing uniform chemisorption of anti-PSA onto the MoS_2 surface. A systematic and statistical study on the capability of the proposed device is presented, and the biological binding events are directly confirmed and characterized through intensive structural and electrical analysis. Our proposed biosensor can reliably detect various PSA concentrations with a limit of 100 fg/mL. Moreover, rigorous theoretical simulations provide a comprehensive understanding of the operating mechanism of the MoS_2 FET biosensors, and further suggests the enhancement of the sensitivity through engineering device design parameters.

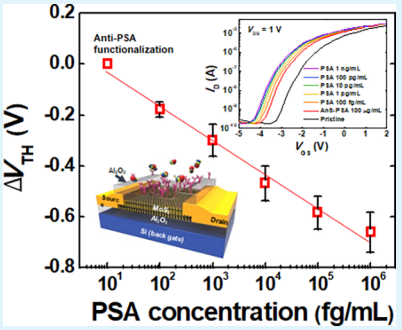

KEYWORDS: *point-of-care diagnostics, MoS_2, biosensor, transistor, nonaqueous*

1. INTRODUCTION

Biosensors allow the ubiquitous acquisition of biological data, and these are in great demand and have become a crucial methodology for point-of-care diagnostics, forensic determination, and other medical applications. Various immunoassay methods have been proposed and studied to provide convenience and patient satisfaction without sacrifcing sensitivity and selectivity. In particular, a fluorescence immunoassay can offer high sensitivity, convenience, and reliability in an aqueous or cellular environment.[1−3] In recent years, there have been massive efforts to use field-effect transistor (FET)-based biosensors as a promising approach for label-free, rapid electrical biomolecule detection due to their low power consumption, scalability into on-chip integration, and low-cost processing.[4−6] Various nanomaterials and nanostructures, including silicon nanowires and carbon nanotubes, have been actively investigated to improve the sensitivity in detecting biomolecules.[7−9] Furthermore, two-dimensional (2-D) nanomaterials, including graphene and transition metal dichalcogenides (TMDs), have shown great potential for ultrasensitive biosensors.[10−13] An atomically thin active layer enables a high surface-to-volume ratio, resulting in a superior charge sensitivity. In particular, the existence of a bandgap in the TMDs unlike the zero-bandgap graphene is critical for the FET-based platform since the binding process at the interface between the 2-D channel and biomolecules induces the carrier transport modulation in 2-D layered materials.[10] Lately, the feasibility of implementing real-time biomolecule detection systems for use in point-of-care diagnostics with MoS_2 FET biosensor was successfully demonstrated by our group.[14]

For the practical use of MoS_2 FET biosensors, greater accuracy and reliability in the operation and diagnostics are of paramount importance. However, thus far, many prior works have largely focused on detection mechanisms, device fabrication, and sensitivity improvement.[10−15] Although various other approaches have been extensively investigated, no studies have reported outstanding results in terms of accuracy and repeatability of biosensors.

In this study, our biosensors are demonstrated to overcome previous limitations and fulfill the requirements mentioned

Received: September 23, 2017
Accepted: November 24, 2017
Published: November 24, 2017

DOI: 10.1021/acsami.7b14479
ACS Appl. Mater. Interfaces 2017, 9, 43490−43497

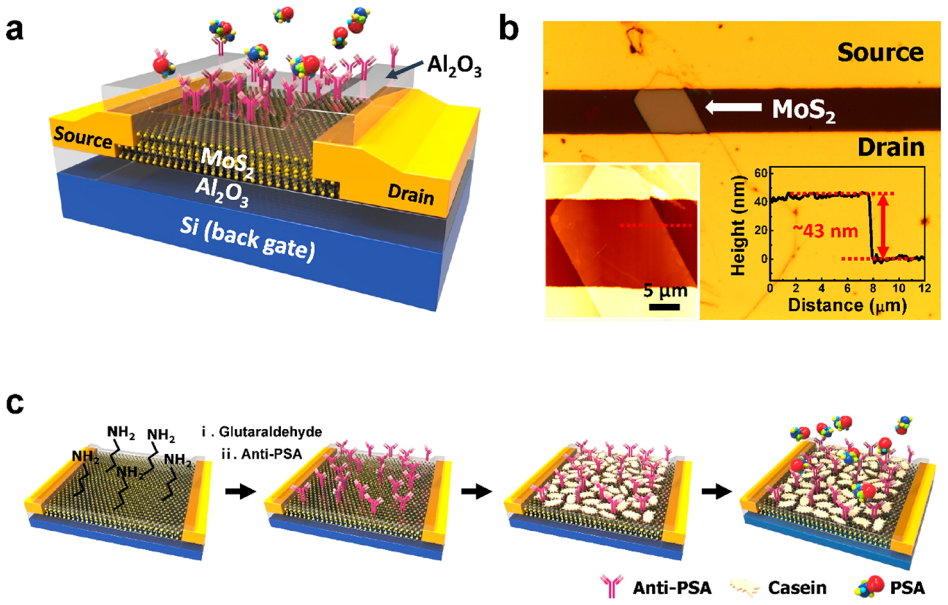

Figure 1. (a) Schematic illustration representing a pseudo-double-gate structure of a MoS_2 biosensor, (b) optical image of the MoS_2 bio-FET with insets representing a tapping-mode AFM image and its thickness profile, and (c) experimental process of a surface chemistry to prepare anti-PSA on MoS_2 surface and its immune reaction with PSA.

above. We present reliable and quantitative detection of prostate cancer antigen (PSA) using the MoS_2 FET sensor in a nonaqueous (i.e., dry-type) environment by reducing the nonspecific molecular binding events and realizing uniform chemisorption of anti-PSA onto the MoS_2 surface. A nonaqueous environment has been considered due to its innately high sensitivity and convenient use, particularly for point-of-care diagnostics.[15] A well-known theory of "pH-memory" in biophysics[16−18] (when the proteins are lyophilized or dried, the ionization state corresponding to the pH of the aqueous solution is retained) espouses the theoretical basis for molecular detection in a nonaqueous environment. It not only shows enormous potential for the MoS_2 FET sensor, but also exhibits excellent reliability and repeatability with the proposed architecture for PSA detection with an ultrahigh sensitivity. To achieve further improvement, we integrated casein as a blocking agent to minimize nonspecific binding during the immuno-reactions. For systematic analyses of the proposed device, Kelvin probe force microscopy (KPFM) and tapping-mode atomic force microscopy (tm-AFM) were used to directly characterize the protein-binding events. Furthermore, we conducted rigorous theoretical simulations to describe our experimental results using a pseudo-double-gate FET model. The capability to perform reliable and quantitative detection of protein markers shows enormous potential to place the proposed MoS_2 FET biosensor into practice as a standard platform.

2. EXPERIMENTAL SECTION

2.1. MoS_2 Bio-FET Fabrication and Measurement. First, a 40 nm thick aluminum oxide (Al_2O_3) gate insulator was deposited via atomic layer deposition on a highly p^+-doped Si wafer. The multilayer MoS_2 was mechanically exfoliated from bulk MoS_2 and transferred onto the gate insulator using transparent adhesive tape. After deposition of Ti/Au (20 nm/100 nm) electrodes via e-beam evaporation, the source and drain (S/D) were formed by photolithography and a conventional lift-off process. To reduce the contact resistance between the S/D electrodes and the channel material, MoS_2 FET was annealed at 200 °C for 2 h with mixed gas (100 sccm of Ar/10 sccm of H_2) in a vacuum chamber. Before deposition of an Al_2O_3 layer (40 nm) used for top passivation, the FET was treated with O_2 plasma at a flow rate of 30 sccm at 150 W for 30 s. Finally, the S/D electrodes was opened by etching with buffer oxide etchant for electrical contact. All electrical measurements were performed using a Keithley 4200-SCS semiconductor parameter analyzer under atmospheric environment.

2.2. Surface Functionalization Process. For surface oxidation, the fabricated device was treated with O_2 plasma at 50 W for 60 s. Then, the device was dipped for 2 h into a 3-aminoproplytriethoysilane (APTES) solution which was composed of ethanol/water (19 mL/1 mL) solution with 0.4 mL of APTES. The APTES-coated device was rinsed in ethanol and blown using nitrogen gas, and baked in a vacuum oven at 120 °C for 5 min. After that, the device was immersed for 2 h into solution containing glutaraldehyde (GA) (4.5 mL), $NaCNBH_4$ (6 mM), and one phosphate buffered saline tablet with deionized (DI) water (200 mL), followed by washing with DI water.

2.3. Anti-PSA Immobilization and Biosensing Process. A concentration of 100 μg/mL of anti-PSA solution (Medix Biochemica) was dropped on the device and stored overnight at 4 °C in order to immobilize the anti-PSA. Then, the device was rinsed with deionized (DI) water and incubated in 1% (w/v) casein blocker (Thermo Fisher Scientific) for 1 h at 4 °C to prevent the nonspecific binding sites. After rinsing the device, PSA detection was started with the following steps. First, five different concentrations of PSA solution (EMD Millipore) from 100 fg/mL to 1 ng/mL were dissolved, and each PSA solution was treated on the device surface for 15 min at room temperature in order, followed by rinsing with DI water.

2.4. AFM and KPFM Measurements. The topology and surface potential measurements for all biomolecule cases were performed using a commercial AFM (MultimodeV, Veeco, CA) at room temperature. A conducting cantilever tip (SCM-PIT, Bruker, CA) was mounted in a tip holder (MMEFCH, Veeco, CA) that is capable of controlling the tip voltage. The surface potential measurements were performed in a lift-mode KPFM.

2.5. Simulation. The role of anti-PSA and PSA in the MoS_2 FET biosensor has been investigated by using self-consistent device simulations based on the nonequilibrium Green's function (NEGF) method within an effective mass approximation. Effective mass of 0.57 was used for multilayer MoS_2.[19] Schottky barrier height between MoS_2 and Ti/Au was assumed to be 0.05 eV.[20] A 20 nm channel is used along with equivalent oxide thickness (EOT) of 17.1 nm for both top

DOI: 10.1021/acsami.7b14479
ACS Appl. Mater. Interfaces 2017, 9, 43490−43497

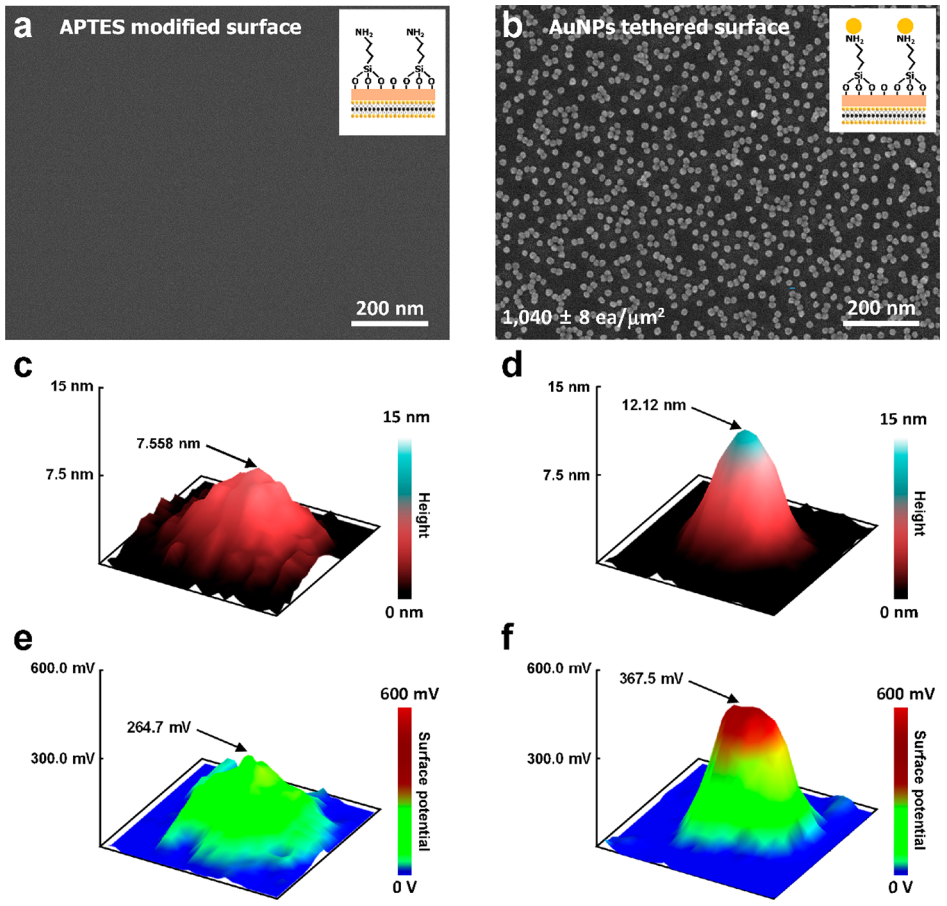

Figure 2. SEM images of the MoS_2 surfaces (a) functionalized with APTES and (b) tethered with AuNPs of 17 nm on the amine surface. AFM images of (c) anti-PSA immobilized on the bio-FET and (d) its complexation with PSA. Topological representation of the surface potential corresponding to the surfaces of (e) anti-PSA and (f) Ab−Ag.

and bottom oxide to determine the effective charge densities at the top oxide surface (N_1 with anti-PSA and $N_2$with PSA). A power supply voltage of V_{DD}= 0.5 V is used. For the discussion of device engineering and optimization, EOT has been varied without changing N_1 and N_2 (considering the same amount of anti-PSA and PSA binding). Although the channel length for the simulation is much shorter than the actual channel of the fabricated device, it has negligible effects within the ballistic transport. Scattering is ignored; however, it would not alter the qualitative results of this study.

3. RESULTS AND DISCUSSION

The conceptual structure of the MoS_2 pseudo-double-gate FET-based biosensor is illustrated in Figure 1a. After fabrication of the MoS_2 FET structure, a 40 nm thick Al_2O_3 was used as a top dielectric since Al_2O_3 allows surface chemistry via APTES and GA[21] in addition to the enhancement of the electrical performance of the device such as high mobility and small hysteresis.[22] The Al_2O_3 top layer was uniformly deposited on the MoS_2 channel surface, and it plays a critical role in high-capacitive coupling with the surface charge of the adsorbed biomolecules. However, as it is widely known, a lack of dangling bonds of MoS_2 disturbs the uniform growth of the oxide layer on its surface directly, which results in undesirable surface morphology and degradation of electrical properties with the top gate dielectric.[23] Therefore, we conducted O_2 plasma treatment prior to Al_2O_3 deposition to compatibilize the MoS_2 top surface with the Al_2O_3. Figure 1b shows the top view of the fabricated pseudo-double-gate bio-FET, observed using optical microscopy and tm-AFM. Since a high field-effect mobility (μ = 30−50 $cm^2\ V^{-1}\ s^{-1}$ on SiO_2/Si substrate)[24,25] is manifested in the 30−45 nm thick MoS_2 flakes, the MoS_2 flakes with this thickness were chosen to construct the bio-FET.

The overall experimental procedure for surface modification to prepare anti-PSA and its immuno-reaction with PSA is schematically illustrated in Figure 1c. The surface of Al_2O_3 allows the formation of covalent bonding with APTES.[21] Anti-PSA was immobilized onto the CHO termini of GA through the well-known lysine and aldehyde reaction. Casein was used as a blocking agent to minimize nonspecific binding during the immuno-reactions. All proteins were included in the phosphate buffer solution (PBS). However, the device was cleaned with DI water (pH ∼ 5) to eliminate the ionized impurities in PBS before taking the electrical measurements.

In order to confirm the efficiency of the surface modification process for anti-PSA immobilization through the APTES treatment, 17 nm gold nanoparticles (AuNPs) were tethered to the amine surface.[26] The surfaces were functionalized with APTES, and the AuNPs were characterized via field emission-scanning electron microscopy (FE-SEM) (Figure 2a,b). Densely distributed AuNPs were observed as shown in Figure 2b with a surface density of 1040 ± 8 ea/μm^2. This confirms the efficient functionalization of the APTES on the Al_2O_3 surface to immobilize the anti-PSA on the surface of Al_2O_3. The dimensions of an immunoglobulin G (IgG) are reported to be 14.5 nm × 4.0 nm × 8.5 nm,[27,28] where the domain size is approximately 7 times smaller than that of the AuNP used in

DOI: 10.1021/acsami.7b14479
ACS Appl. Mater. Interfaces 2017, 9, 43490−43497

this study. Assuming that the APTES self-assembled monolayer was ideally ordered on the oxide surface, the total number of the immobilized anti-PSAs can be calculated to be 7 times more than that of AuNPs.

For an in-depth study of the immobilization of anti-PSA and its immuno-reaction with PSA on MoS_2 bio-FET, tm-AFM was employed to visualize the structure of the biomolecules at a single molecular level. The AFM image of an anti-PSA and its complexation with PSA (Ab−Ag) are shown in Figure 2c,d, respectively. As shown in Figure 2c, the height of the single anti-PSA was measured at 7.558 nm, which is almost identical to the upright standing height of the IgG.[27,29] To comprehend the characteristics of immobilized anti-PSAs, the Gaussian-distributed height histogram has been plotted in Figure S1, exhibiting the average height of 7.334 nm. This result denotes that the proposed MoS_2 bio-FET contains more well-oriented anti-PSAs with the free PSA binding regions upward, as shown in the right inset of Figure S1.[27,28] The proper orientation of the anti-PSA was controlled by the formation of covalent linkages on the sensor surface through APTES and GA. The immobilized anti-PSA structure with free binding regions is pivotal for active specific binding with PSA, reinforcing the sensitivity and reproducibility in contrast to the random immobilization. The proposed MoS_2 bio-FET is intended for further improvement of the orientation in future studies by applying protein A or protein G, which fashions the covalent bonds on the device surface following binding to the heavy chain of the antibody.[29] After the anti-PSA was immobilized, the device was incubated in a PSA solution, and a height of 12.12 nm was measured, as shown in Figure 2d. Considering that most of the anti-PSA, which can create Ab−Ag complexation, is in good orientation and the molecular weight of the PSA is appropriately 26−28 kDa,[30,31] these results provide evidence of a docking reaction between anti-PSA and PSA. In addition, the experimentally characterized lateral dimension of anti-PSA and Ab−Ag is perceived to be much larger than their true value due to the AFM tip broadening.[32]

KPFM was used to characterize not only the molecular binding behavior but also the binding-induced surface potential variation, considering the correlation between the binding molecules and the charge distribution on the MoS_2 channel. The measured surface potential of the single anti-PSA is presented in Figure 2e. The surface potential of anti-PSA increases from sub-millivolt for the bare surface to 264.7 mV. This positive potential of anti-PSA is attributed to its higher isoelectric point (pI ∼ 7.8) than the pH (∼5) for this measurement.[15] In our previously reported study, the surface potential of anti-PSA was estimated to be more than 200 mV under optimal conditions where no aggregation occurred,[33] which is in good agreement with the current measurement result. Likewise, the surface potential of Ab−Ag was measured with a significant increase in the value of 367.5 mV (Figure 2f) due to its complexation with positively charged PSA. The pI of PSA is ∼6.9,[34−36] indicating that the PSA molecule is positively charged at the pH (∼5) of this measurement. The corresponding statistic distribution profiles of anti-PSA and Ab−Ag are presented in Figure S2. A theoretical study will be provided later, but it should be mentioned here that the positive surface potential induced by the attachment of the biomolecules onto the dielectric layer generates a field gating effect, which induces a significant change of carrier density inside the MoS_2 channel.[37,38] This sensing mechanism can be interpreted as a pseudo-double-gate model representing the potential of the biomolecules attached to the top dielectric surface which controls the current behavior and furthers the threshold voltage (V_{TH}) shift of the MoS_2 bio-FET with a back gate voltage sweep.[39,40]

The electrical characteristics were inspected to authenticate the hypothesis and the behavior of the biosensor with respect to the positive molecular charge of the anti-PSA and PSA immobilized on the surface of the biosensor. The transfer curves of the MoS_2 bio-FET before and after immobilization of the positively charged anti-PSA and positively charged PSA were depicted in Figure 3a,b, respectively. When the MoS_2 FETs surface was functionalized with APTES and GA, the protein immobilization time and temperature, the pH of the PBS buffer containing proteins, and the washing condition were equally maintained. There was no additional process to immobilize PSA because the amino groups of PSA are also capable of forming covalent linkages with the aldehyde functionalized surface.[41] The drain current (I_D) was measured as a function of the gate voltage (V_{GS}) from −7 to 5 V at the drain voltage (V_{DS}) of 1 V. A significant increase of I_D was observed at all V_{GS} values when the positively charged anti-PSA or PSA was immobilized. The direction of the corresponding V_{TH} shift was found to be negative, which can be understood from $\Delta V_{TH} = -Q_F/C_O$, where Q_F represents the effective charges that can induce the change in the conductivity of the MoS_2 channel and C_O represents the total capacitance of the dielectric layer. Consequently, the binding of anti-PSA or PSA offers a positive gating effect to the MoS_2 channel, leading to a

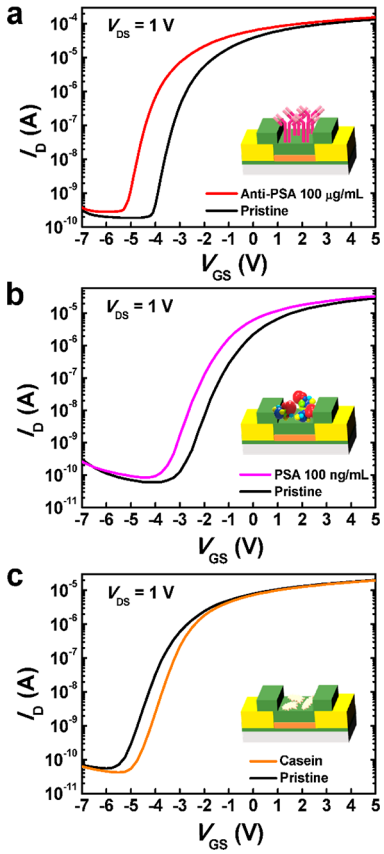

Figure 3. Shifts in the transfer curves for the MoS_2 bio-FET immobilized with (a) anti-PSA of 100 μg/mL, (b) PSA of 100 ng/mL and, (c) casein of 1% (w/v).

DOI: 10.1021/acsami.7b14479
ACS Appl. Mater. Interfaces 2017, 9, 43490−43497

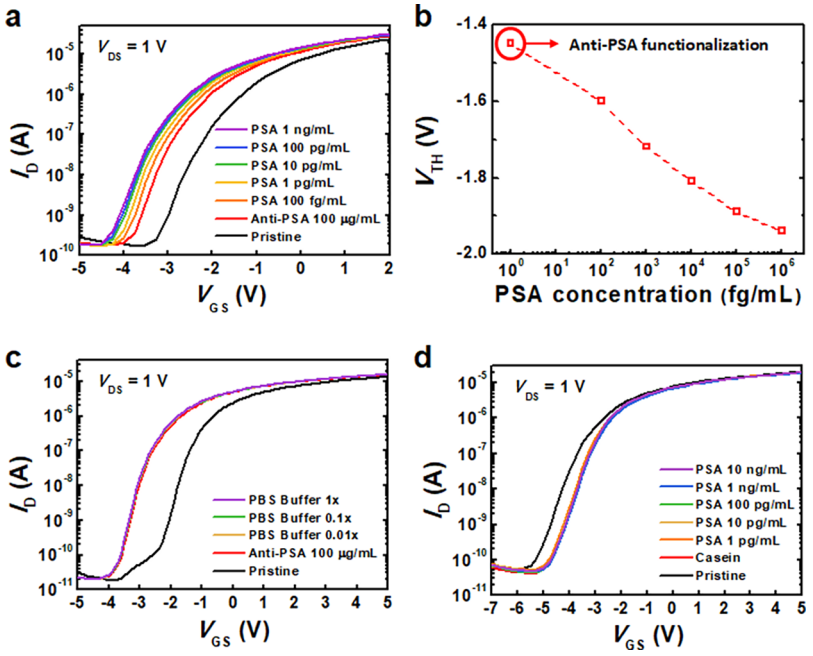

Figure 4. (a) Transfer characteristics with PSA concentrations from 100 fg/mL to 1 ng/mL on the anti-PSA-immobilized MoS_2 bio-FET, (b) plot of V_{TH} against PSA concentrations, (c) transfer curves of the MoS_2 bio-FET when different concentrations of PBS buffer solution were used, and (d) transfer behavior of the bio-FET unimmobilized with anti-PSA onto which different concentrations of PSA were added.

negative shift of V_{TH}. In contrast, the introduction of casein, whose charge is estimated to be negative due to its lower pI (~4.6) than the pH of DI water, induced a current decrease and the positive shift of V_{TH}, as shown in Figure 3c. These results demonstrate the potential of the double gate bio-FET for distinguishing opposed charged biomolecules in a dry environment. Notably, the pH memory theory can be an excellent theoretical tool for highly accurate and reproducible biosensor operation.

The label-free detection of the MoS_2 bio-FET in a nonaqueous environment was conducted by measuring I_D–V_{GS} at several biodetection steps. Figure 4a presents the transfer curves of anti-PSA-modified MoS_2 bio-FET with respect to various concentrations of PSA. The immobilization of anti-PSA resulted in a current increase contributing to a negative V_{TH} shift, which is consistent with Figure 3a. After the anti-PSA immobilization, we could not observe a noticeable current degradation even with negatively charged caseins due to extremely low density compared to that of immobilized anti-PSA. The specific binding of positively charged PSA increased the I_D of the bio-FET stepwise with an increased concentration. Figure 4b shows the calibrated sensor responses of V_{TH} variation with different PSA concentrations. Notably, we were able to detect PSA as low as 100 fg/mL, which is much lower than the previously reported value (1 pg/mL).[15] The major contributing factor for this superior detection capability is the unique method used to prepare anti-PSA on the MoS_2 sensing surface. In contrast to the physically absorbed anti-PSA in the previous report,[15] we adopted a chemical surface modification, which provided more stable immobilization as well as a good orientation of the anti-PSA to achieve the highest PSA binding. However, unexpectedly, the V_{TH} variation according to the PSA concentrations (Figure 4b) did not reveal a typical s-shape,[42] representing the sensitivity saturation at the lowest and highest concentrations. It suggested that the limit of detection (LOD) of the MoS_2 bio-FET could be reduced under 100 fg/mL, leading to the potential of the MoS_2 bio-FET for ultrasensitive biosensors. The corresponding output characteristics were plotted in Figure S3. I_D was measured by sweeping V_{DS} from 0 to 5 V, exhibiting that I_D was increased due to the negative shift of V_{TH} with anti-PSA immobilization and PSA detection.

Several control experiments were conducted to verify that the observed V_{TH} shifts are due to the specific binding of PSA with anti-PSA. The electrical response of the MoS_2 bio-FET for various diluted PBS buffer solutions was examined to confirm the effect of the ionic strength in the MoS_2 biosensor as depicted in Figure 4c. The MoS_2 bio-FET functionalized with anti-PSA was soaked in PBS buffer for 15 min and then was dried out to conduct electrical measurements. The experimental consequences show no noticeable change in current with the addition of 1× , 0.1× , and 0.01× PBS buffer on the anti-PSA-immobilized sample. In contrast to the nonaqueous measurement environment, the electrical performance of the bio-FET under a bath solution is extremely sensitive to the ionic concentration of the buffer solution.[43] The detection of charged molecules under a high ionic strength buffer is disturbed by the ionic screening effect.[36] Furthermore, the large leakage current induced by the solution ions is an inherent limitation that reduces the sensitivity of aqueous-type biosensors. In a nonaqueous environment of our experiment, the above-mentioned problems hindering the sensitivity and reproducibility of biosensors could be excluded, and these experimental consequences imply that our measurement mechanism is substantially robust and trustworthy for use in commercial FET-based diagnostic applications.

Figure 4d unequivocally demonstrates a nonspecific reaction of the PSA to casein and bare MoS_2 surface without anti-PSA. The addition of PSA solutions to unfunctionalized MoS_2 bio-FET did not lead to a significant change in the transfer curves. There is little nonspecific binding that is unrecognized from the electrical signals.

DOI: 10.1021/acsami.7b14479
ACS Appl. Mater. Interfaces 2017, 9, 43490–43497

In addition, the selectivity of our MoS_2 bio-FET for target PSA was evaluated by comparing the sensing signal variations of samples with several potential interfering proteins, IgG, and human serum albumin (HSA). As shown in Figure S4, the threshold voltage shift (ΔV_{TH}) values after treatment of IgG (10 ng/mL) and HSA (10 ng/mL) without PSA were clearly distinguished from that of the PSA (1 ng/mL) sample. Also, small differences of ΔV_{TH} were observed in samples containing PSA (1 ng/mL) mixed with IgG (10 ng/mL) or HSA (10 ng/mL) compared with the sample of only PSA, but they could be negligible for PSA detection.

Figure 5 reveals average sensing responses of seven different MoS_2 bio-FETs to various PSA concentrations. The ΔV_{TH} values were obtained from the device shown in Figure 4a, and an additional six devices as presented in Figure S5. Although seven sensors have a noticeable difference in V_{TH} and I_D, Figure 5 exhibits that ΔV_{TH} with PSA binding relative to the I_D-V_{GS} only with anti-PSA of each device did not deviate significantly from the mean value (standard error from the average ΔV_{TH} were under 9%). More specifically, the data points of average ΔV_{TH} agreed well with the linearly fitted line, ensuring great sensing linearity as well as reliability. In most FET-based biosensor studies, the statistical analysis was rarely achieved because it is difficult to ensure the reproducibility of biosensors. Therefore, our approach offers an intriguing chance for non-aqueous-type biosensors.

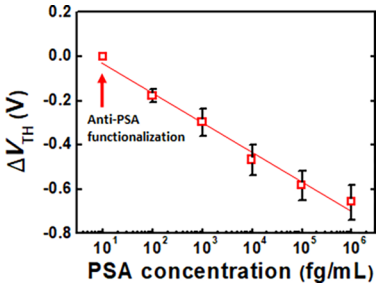

Figure 5. Average of ΔV_{TH} of seven MoS_2 FET-based biosensors at various concentrations of PSA, relative to the I_D-V_{GS} only with anti-PSA.

The clinical applicability of our biosensor can be investigated by conducting PSA detection in real human serum. The electrical responses of MoS_2 bio-FET with various PSA concentrations in 10-fold diluted human serum were presented in Figure S6. The LOD of MoS_2 bio-FET in diluted human serum was successfully extracted to 100 fg/mL, which is the same value as in the PBS condition. This result indicated that MoS_2 bio-FETs have great potential as a real diagnostic device.

In order to develop in-depth understanding of the sensitivity of the device, numerical simulations have been performed using the NEGF method. The role of anti-PSA and PSA attached to the top oxide is mimicked by introducing additional positive charge densities (N) at the surface. Figure 6a shows the V_{TH} shifts relative to the pristine device by increasing N with a fixed equivalent oxide thickness ($EOT = t_{Al_2O_3}\frac{\kappa_{SiO_2}}{\kappa_{Al_2O_3}}$) of the top oxide ($EOT_{TOP}$ = 17.1 nm; blue lines), which is equivalent to the EOT in the actual fabricated device. The values of N_1 and N_2 ($N_1 = 2.6 \times 10^{11}$ cm^{-2}; $N_2 = 4.2 \times 10^{11}$ cm^{-2}) are determined to match the experimental V_{TH} shifts of −0.31 and −0.5 V with anti-PSA and PSA binding (100 fg/mL), respectively, from the I_D-V_{GS} of the pristine device. Anti-PSA and PSA on the top oxide behave like a secondary gate with positive bias, which

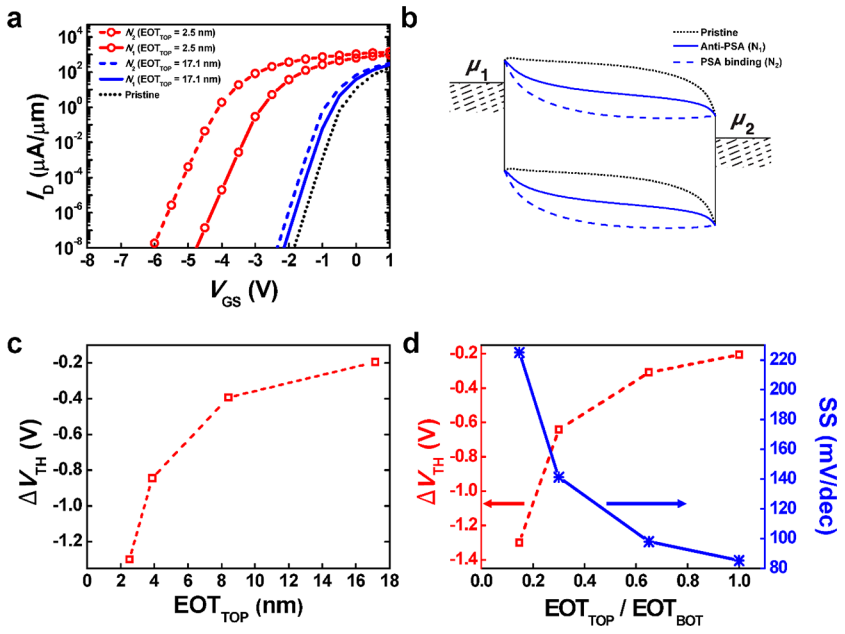

Figure 6. (a) Simulated I_D-V_{GS} characteristics of multilayer MoS_2 biosensor for a pristine device (black dotted line) and the cases with two different positive charge densities on the top oxide surface, $N_1 = 2.6 \times 10^{11}$ cm^{-2} (blue —) and $N_2 = 4.2 \times 10^{11}$ cm^{-2} (blue ---), commonly with an EOT_{TOP} of 17.1 nm (same as EOT of the fabricated device). The charge densities of N_1 and N_2 are determined such that the V_{TH} shift in experiments can be reproduced for anti-PSA and PSA binding (100 fg/mL), respectively. The red — (---) with ○ is for N_1 (N_2) with a reduced EOT_{TOP} of 2.5 nm. (b) Energy band diagram for a pristine device (black ···) and the cases with N_1 (blue —) and N_2 (blue ---). $\mu_{1,2}$ values are electrochemical potentials at the source and the drain, respectively. (c) ΔV_{TH} with PSA binding (N_2) as a function of EOT_{TOP} for a fixed EOT_{BOT} of 17.1 nm. (d) ΔV_{TH} (□; left axis) and subthreshold swing (SS) of devices (*; right axis) as a function of EOT_{TOP}/EOT_{BOT}, where EOT_{BOT} is varied with a fixed EOT_{TOP} of 2.5 nm.

DOI: 10.1021/acsami.7b14479
ACS Appl. Mater. Interfaces 2017, 9, 43490−43497

lowers the potential in the channel region as depicted in the energy band diagram shown in Figure 6b.

Given our understanding of the roles of anti-PSA and PSA with a fixed EOT_{TOP}, next we change device parameters such as EOT to enhance ΔV_{TH} (which is defined as V_{TH} shift with PSA binding of N_2 relative to the I_D-V_{GS} with anti-PSA of N_1) for a better sensitivity. In Figure 6a, it can be observed that the V_{TH} shift of the MoS_2 biosensor can be significantly improved by using a thinner EOT for the top oxide. With an EOT_{TOP} = 2.5 nm (red lines with ○), ΔV_{TH} can be as large as −1.3 V, which is a 6.7× improvement as compared to the value with EOT_{TOP} = 17.1 nm (−0.2 V, blue lines). Figure 6c exhibits the enhancement of ΔV_{TH} with thinner EOT_{TOP}, suggesting further optimization of MoS_2 biosensors with device parameters.

Bottom gate oxide thickness is another parameter we should consider for optimization, as the overall performance of nanoscale devices is, in general, largely affected by gate oxide. We have varied EOT_{BOT} from 17.1 nm down to 2.5 nm with a fixed EOT_{TOP} of 2.5 nm. Figure 6d shows the variation of ΔV_{TH} as a function of EOT_{TOP}/EOT_{BOT}. As the ratio of EOT_{TOP}/EOT_{BOT} increases from 0.15 to 1, the device becomes less sensitive to the same amount of PSA, as the electrostatic control by the bottom gate becomes more efficient and the secondary gate effect becomes relatively weaker. Although such a case is undesirable for practical sensing applications, energy can be saved significantly by using a low power supply voltage since the subthreshold swing (SS) of the device improves with the EOT_{TOP}/EOT_{BOT} ratio as shown by the asterisks (right axis) in Figure 6d. Therefore, it is suggested that both top and bottom oxide should be simultaneously engineered to meet the requirements in sensitivity and power consumption of the sensors.

4. CONCLUSION

In summary, we have demonstrated a MoS_2 FET biosensor that provides reliable and quantitative detection of biomarker in a nonaqueous environment by excluding nonspecific binding and thus realizing uniform chemisorption of biomolecules on the MoS_2 surface. The proposed architecture and process scheme allow the MoS_2 FET biosensor to detect various concentrations of PSA as low as 100 fg/mL with a standard error under 9%. A statistical study as well as control experiments confirm that the high sensitivity and reliability are obtained by the specific binding events of anti-PSA. It is shown through the intensive structural and electrical characterization of the binding process that the uniform chemisorption and good orientation of anti-PSA can be achieved by casein treatment. Moreover, theoretical simulation using the NEGF method suggests that further optimization of the device structure can result in a more sensitive and power-efficient MoS_2 FET biosensor. Our experimental and simulation results show that the proposed architecture provides excellent reproducibility and ultrahigh sensitivity for the dry-type MoS_2 biosensor and thus has great potential for point-of-care diagnostic applications.

■ ASSOCIATED CONTENT

Supporting Information

The Supporting Information is available free of charge on the ACS Publications website at DOI: 10.1021/acsami.7b14479.

Statistically distributed height profile of anti-PSA (Figure S1) and surface potential profile of anti-PSA and Ab−Ag (Figure S2), response of output curves with biodetection steps (Figure S3), PSA detection of MoS_2 bio-FETs with some interfering proteins (Figure S4), and additional PSA-sensing results of MoS_2 bio-FETs (Figure S5) (PDF)

■ AUTHOR INFORMATION

Corresponding Authors

*E-mail: intel0616@gmail.com (S.K.).
*E-mail: youngki.yoon@uwaterloo.ca (Y.Y.).
*E-mail: gwyoo@ssu.ac.kr (G.Y.).

ORCID

Gyuchull Han: 0000-0002-4955-208X
Sunkook Kim: 0000-0003-1747-4539

Notes

The authors declare no competing financial interest.

■ ACKNOWLEDGMENTS

This research was supported in part by the National Research Foundation of Korea (2015R1A1A1A05027488, 2014M3A9D7070732, 2017R1CB5017470). This research was partially supported by the Commercializations Promotion Agency for R&D Outcomes (COMPA) funded by the Ministry of Science, ICT, and Future Planning (MISP). This work was supported in part by NSERC Discovery Grant (RGPIN-05920-2014). G.H. acknowledges the financial support by NSERC Canada Graduate Scholarships Program and WIN Nanofellowship. H.P., G.H., and S.W. L. contributed equally to this work.

■ REFERENCES

(1) Yao, J.; Yang, M.; Duan, Y. Chemistry, Biology, and Medicine of Fluorescent Nanomaterials and Related Systems: New Insights into Biosensing, Bioimaging, Genomics, Diagnostics, and Therapy. *Chem. Rev.* **2014**, *114* (12), 6130−6178.

(2) Pei, H.; Zhu, S.; Yang, M.; Kong, R.; Zheng, Y.; Qu, F. Graphene Oxide Quantum Dots@ Silver Core−Shell Nanocrystals as Turn-on Fluorescent Nanoprobe for Ultrasensitive Detection of Prostate Specific Antigen. *Biosens. Bioelectron.* **2015**, *74*, 909−914.

(3) Kong, R.-M.; Ding, L.; Wang, Z.; You, J.; Qu, F. A Novel Aptamer-Functionalized MoS_2 Nanosheet Fluorescent Biosensor for Sensitive Detection of Prostate Specific Antigen. *Anal. Bioanal. Chem.* **2015**, *407* (2), 369−377.

(4) Bergveld, P. Development of an Ion-Sensitive Solid-State Device for Neurophysiological Measurements. *IEEE Trans. Biomed. Eng.* **1970**, *BME-17* (1), 70−71.

(5) Wang, J. Electrochemical Biosensors: towards Point-of-care Cancer Diagnostics. *Biosens. Bioelectron.* **2006**, *21* (10), 1887−1892.

(6) Zheng, G.; Patolsky, F.; Cui, Y.; Wang, W. U.; Lieber, C. M. Multiplexed Electrical Detection of Cancer Markers with Nanowire Sensor Arrays. *Nat. Biotechnol.* **2005**, *23* (10), 1294−1301.

(7) Shoorideh, K.; Chui, C. O. On the Origin of Enhanced Sensitivity in Nanoscale FET-Based Biosensors. *Proc. Natl. Acad. Sci. U. S. A.* **2014**, *111* (14), 5111−5116.

(8) Yang, W.; Ratinac, K. R.; Ringer, S. P.; Thordarson, P.; Gooding, J. J.; Braet, F. Carbon Nanomaterials in Biosensors: Should You Use Nanotubes or Graphene? *Angew. Chem., Int. Ed.* **2010**, *49* (12), 2114−2138.

(9) Cui, Y.; Wei, Q.; Park, H.; Lieber, C. M. Nanowire Nanosensors for Highly Sensitive and Selective Detection of Biological and Chemical Species. *Science* **2001**, *293* (5533), 1289−1292.

(10) Sarkar, D.; Liu, W.; Xie, X.; Anselmo, A. C.; Mitragotri, S.; Banerjee, K. MoS_2 Field-Effect Transistor for Next-Generation Label-free Biosensors. *ACS Nano* **2014**, *8* (4), 3992−4003.

(11) Kalantar-zadeh, K.; Ou, J. Z.; Daeneke, T.; Strano, M. S.; Pumera, M.; Gras, S. L. Two-Dimensional Transition Metal

DOI: 10.1021/acsami.7b14479
ACS Appl. Mater. Interfaces 2017, 9, 43490−43497

Dichalcogenides in Biosystems. *Adv. Funct. Mater.* **2015**, *25* (32), 5086−5099.
(12) Kalantar-zadeh, K.; Ou, J. Z. Biosensors Based on Two-Dimensional MoS_2. *ACS Sens.* **2016**, *1* (1), 5−16.
(13) Gan, X.; Zhao, H.; Quan, X. Two-dimensional MoS_2: A Promising Building Block for Biosensors. *Biosens. Bioelectron.* **2017**, *89*, 56−71.
(14) Yoo, G.; Park, H.; Kim, M.; Song, W. G.; Jeong, S.; Kim, M. H.; Lee, H.; Lee, S. W.; Hong, Y. K.; Lee, M. G.; et al. Real-time Electrical Detection of Epidermal Skin MoS_2 Biosensor for Point-of-care Diagnostics. *Nano Res.* **2017**, *10* (3), 767−775.
(15) Lee, J.; Dak, P.; Lee, Y.; Park, H.; Choi, W.; Alam, M. A.; Kim, S. Two-Dimensional Layered MoS_2 Biosensors Enable Highly Sensitive Detection of Biomolecules. *Sci. Rep.* **2015**, *4*, 7352.
(16) Costantino, H. R.; Griebenow, K.; Langer, R.; Klibanov, A. M. On the pH Memory of Lyophilized Compounds Containing Protein Functional Groups. *Biotechnol. Bioeng.* **1997**, *53* (3), 345−348.
(17) Meyers, R. A. *Molecular Biology and Biotechnology: A Comprehensive Desk Reference*; John Wiley & Sons: Germany, 1995.
(18) Zaks, A.; Klibanov, A. M. Enzyme-Catalyzed Processes in Organic Solvents. *Proc. Natl. Acad. Sci. U. S. A.* **1985**, *82* (10), 3192−3196.
(19) Zahid, F.; Liu, L.; Zhu, Y.; Wang, J.; Guo, H. A Generic Tight-Binding Model for Monolayer, Bilayer and Bulk MoS_2. *AIP Adv.* **2013**, *3* (5), 052111.
(20) Das, S.; Chen, H.-Y.; Penumatcha, A. V.; Appenzeller, J. High Performance Multilayer MoS_2 Transistors with Scandium Contacts. *Nano Lett.* **2013**, *13* (1), 100−105.
(21) Wang, X.; Chen, Y.; Gibney, K. A.; Erramilli, S.; Mohanty, P. Silicon-Based Nanochannel Glucose Sensor. *Appl. Phys. Lett.* **2008**, *92* (1), 013903.
(22) Kufer, D.; Konstantatos, G. Highly Sensitive, Encapsulated MoS_2 Photodetector with Gate Controllable Gain and Speed. *Nano Lett.* **2015**, *15* (11), 7307−7313.
(23) Yang, J.; Kim, S.; Choi, W.; Park, S. H.; Jung, Y.; Cho, M.-H.; Kim, H. Improved Growth Behavior of Atomic-Layer-Deposited High-k Dielectrics on Multilayer MoS_2 by Oxygen Plasma Pretreatment. *ACS Appl. Mater. Interfaces* **2013**, *5* (11), 4739−4744.
(24) Bao, W.; Cai, X.; Kim, D.; Sridhara, K.; Fuhrer, M. S. High Mobility Ambipolar MoS_2 Field-Effect Transistors: Substrate and Dielectric Effects. *Appl. Phys. Lett.* **2013**, *102* (4), 042104.
(25) Yang, R.; Wang, Z.; Feng, P. X.-L. Electrical Breakdown of Multilayer MoS_2 Field-Effect Transistors with Thickness-Dependent Mobility. *Nanoscale* **2014**, *6* (21), 12383−12390.
(26) Leff, D. V.; Brandt, L.; Heath, J. R. Synthesis and Characterization of Hydrophobic, Organically-Soluble Gold Nanocrystals Functionalized with Primary Amines. *Langmuir* **1996**, *12* (20), 4723−4730.
(27) Tan, Y. H.; Liu, M.; Nolting, B.; Go, J. G.; Gervay-Hague, J.; Liu, G.-y. A Nanoengineering Approach for Investigation and Regulation of Protein Immobilization. *ACS Nano* **2008**, *2* (11), 2374−2384.
(28) Trilling, A. K.; Beekwilder, J.; Zuilhof, H. Antibody Orientation on Biosensor Surfaces: A Minireview. *Analyst* **2013**, *138* (6), 1619−1627.
(29) Dutta, P.; Sawoo, S.; Ray, N.; Bouloussa, O.; Sarkar, A. Engineering Bioactive Surfaces with Fischer Carbene Complex: Protein A on Self-Assembled Monolayer for Antibody Sensing. *Bioconjugate Chem.* **2011**, *22* (6), 1202−1209.
(30) Gabriela De Angelis, M.; Rittenhouse, H. G.; Stephen, D.; Mikolajczyk, B.; Shamel, L. B.; Semjonow, A. Twenty Years of PSA: from Prostate Antigen to Tumor Marker. *Rev. Urol* **2007**, *9* (3), 113−123.
(31) Lee, S.-M.; Hwang, K. S.; Yoon, H.-J.; Yoon, D. S.; Kim, S. K.; Lee, Y.-S.; Kim, T. S. Sensitivity Enhancement of a Dynamic Mode Microcantilever by Stress Inducer and Mass Inducer to Detect PSA at Low Picogram Levels. *Lab Chip* **2009**, *9* (18), 2683−2690.
(32) Keller, D. Reconstruction of STM and AFM Images Distorted by Finite-Size Tips. *Surf. Sci.* **1991**, *253* (1−3), 353−364.
(33) Kim, M. H.; Park, H.; Lee, H.; Nam, K.; Jeong, S.; Omkaram, I.; Yoon, D. S.; Lee, S. Y.; Kim, S.; Lee, S. W. Research Update: Nanoscale Surface Potential Analysis of MoS_2 Field-Effect Transistors for Biomolecular Detection Using Kelvin Probe Force Microscopy. *APL Mater.* **2016**, *4* (10), 100701.
(34) Wang, M.; Kuriyama, M.; Papsidero, L.; Loor, R.; Valenzuela, L.; Murphy, G.; Chu, T. Prostate Antigen of Human Cancer Patients. *Methods Cancer Res.* **1982**, *19*, 179−197.
(35) Kim, A.; Ah, C. S.; Yu, H. Y.; Yang, J.-H.; Baek, I.-B.; Ahn, C.-G.; Park, C. W.; Jun, M. S.; Lee, S. Ultrasensitive, Label-free, and Real-time Immunodetection Using Silicon Field-Effect Transistors. *Appl. Phys. Lett.* **2007**, *91* (10), 103901.
(36) Huang, Y.-W.; Wu, C.-S.; Chuang, C.-K.; Pang, S.-T.; Pan, T.-M.; Yang, Y.-S.; Ko, F.-H. Real-time and Label-free Detection of the Prostate-Specific Antigen in Human Serum by a Polycrystalline Silicon Nanowire Field-Effect Transistor Biosensor. *Anal. Chem.* **2013**, *85* (16), 7912−7918.
(37) Gao, X. P.; Zheng, G.; Lieber, C. M. Subthreshold Regime Has the Optimal Sensitivity for Nanowire FET Biosensors. *Nano Lett.* **2010**, *10* (2), 547−552.
(38) Sarkar, D.; Banerjee, K. Proposal for Tunnel-Field-Effect-Transistor as Ultra-Sensitive and Label-free Biosensors. *Appl. Phys. Lett.* **2012**, *100* (14), 143108.
(39) Lee, G.-H.; Cui, X.; Kim, Y. D.; Arefe, G.; Zhang, X.; Lee, C.-H.; Ye, F.; Watanabe, K.; Taniguchi, T.; Kim, P.; Hone, J. Highly Stable, Dual-Gated MoS_2 Transistors Encapsulated by Hexagonal Boron Nitride with Gate-Controllable Contact, Resistance, and Threshold Voltage. *ACS Nano* **2015**, *9* (7), 7019−7026.
(40) Seok, M. J.; Choi, M. H.; Mativenga, M.; Geng, D.; Kim, D. Y.; Jang, J. A Full-Swing a-IGZO TFT-Based Inverter with a Top-Gate-Bias-Induced Depletion Load. *IEEE Electron Device Lett.* **2011**, *32* (8), 1089−1091.
(41) Acharya, A. S.; Manning, J. M. Reaction of Glycolaldehyde with Proteins: Latent Crosslinking Potential of Alpha-Hydroxyaldehydes. *Proc. Natl. Acad. Sci. U. S. A.* **1983**, *80* (12), 3590−3594.
(42) Reiner-Rozman, C.; Kotlowski, C.; Knoll, W. Electronic Biosensing with Functionalized rGO FETs. *Biosensors* **2016**, *6* (2), 17.
(43) Lambrechts, M.; Sansen, W. *Biosensors: Microelectrochemical Devices*; CRC Press: U.K., 1992.

DOI: 10.1021/acsami.7b14479
ACS Appl. Mater. Interfaces 2017, 9, 43490−43497